High-resolution threshold photodetachment spectroscopy of OH^-

Jim R. Smith, Joseph B. Kim, and W. C. Lineberger
Department of Chemistry and Biochemistry and JILA, University of Colorado and National Institute of Standards and Technology, Boulder, Colorado 80309
(Received 26 September 1996)

Relative photodetachment cross sections for rotational thresholds of the hydroxide anion were measured using a coaxial laser-ion beam spectrometer. The thresholds correspond to transitions from the $J=1$ and $J=2$ states of $X\ ^1\Sigma^+$ OH^- to the $J=3/2$ state of $X\ ^2\Pi_{3/2}$ OH. Best fits of the data give cross sections that scale with energy above threshold as $(E-E_{th})^{0.18\pm0.06}$ and $(E-E_{th})^{0.21\pm0.05}$ for the two thresholds, respectively. This non-Wigner law energy dependence of the cross section results from the long-range r^{-2} interaction between the dipole and the departing electron. Experimental results were compared with the predictions of a strong-coupling model of charge-dipole interaction devised by Engelking and good qualitative agreement was observed. When the resolution and range of the data for transitions that terminate in the lower Λ-doublet component is such that the Λ-doublet splitting is resolved, one observes the $(E-E_{th})^{1/2}$ behavior predicted by the Wigner law. This result is explained in terms of the effect of the Λ doubling upon the r^{-2} charge-dipole interaction. From the threshold frequencies, an OH electron affinity of 14 741.02(3) cm^{-1} was determined. [S1050-2947(97)04803-8]

PACS number(s): 33.80.Eh

I. INTRODUCTION

Laser photodetachment threshold spectroscopy of negative ions is a well-known technique [1,2] for determining information about the dynamics of the photodetachment process as well as for obtaining spectroscopic information. The photodetachment of OH^- has a long history and an excellent summary of the early history has been given by Schulz *et al.* [3]. In addition, OH^- was one of the first negative ions to be observed in the gas phase by direct absorption spectroscopy [4]. The energy dependence of the photodetachment cross section for energies just above a channel opening, referred to as the threshold law, provides information about the interaction between the departing electron and the remaining neutral species. In addition, the frequencies of the channel openings (thresholds) can provide a wealth of spectroscopic information about the initial ionic species as well as the neutral species produced during the process. In this work, laser photodetachment threshold spectroscopy was performed on OH^-, and the relative photodetachment cross sections for three thresholds were measured under high resolution.

In 1948, Wigner derived expressions for the behavior of cross sections near the thresholds for various processes that produce pairs of particles, in terms of the long-range interactions between the particles [5]. The derivation predicts and experiments have confirmed [3,6] that it is the longest-range interactions (forces) that determine the threshold law. Experimental measurements of the near-threshold photodetachment cross section thus can provide information about the long-range interactions between the particles produced by the process. Since a slow-moving, near-threshold electron spends a long time under the influence of any long-range potentials as it is departing, it is those potentials rather than any shorter-range ones that govern the threshold behavior.

For the photodetachment of an atomic negative ion, the longest-range interaction that is present between the atom and the departing electron is the $\ell(\ell+1)/r^2$ centrifugal potential due to the departing electron's angular momentum. The Wigner threshold law for this process is $\sigma\sim k^{2\ell+1}$, or, equivalently, $\sigma\sim(E-E_{th})^{\ell+1/2}$, where k and ℓ are the linear and angular momenta of the detached electron, E is the photon energy, and E_{th} is the threshold energy. The centrifugal potential is combined with any shorter-range potentials that are present to give an effective potential that is then used in the standard approach to solving the Schrödinger equation for this problem [7]. This effective potential then contains a barrier that a nascent photodetached electron in the inner region of the potential must tunnel through in order to become a free particle. If two partial waves (values of l) are accessible, then a near-threshold electron will have the lowest angular momentum value possible, since this will produce the lowest barrier for tunneling. Experiments have confirmed that Wigner's law holds for atomic negative ions [8–11].

The Wigner law holds only as the limit threshold is approached, or, in other words, as $k\rightarrow0$, and contains no information about the range of validity of the threshold law. The photodetachment cross section can be described by a power-series expansion in k [12]. The threshold law is then given by the first term in the expansion, with higher-order terms becoming more important as k increases. Interaction potentials that have a shorter range than the centrifugal potential, such as those arising from the polarizability or quadrupole moment of the neutral, affect the higher-order terms of the expansion but do not change the leading term.

The Wigner law was originally applied to the photodetachment of atomic anions. However, Geltman derived a threshold law for photodetachment from a nonpolar diatomic anion [13], while Reed *et al.* derived results for polyatomic molecular anions [14]. The threshold laws that they derived are consistent with the Wigner law, but symmetry arguments are used to determine the lowest partial wave available to the detached electron.

For photodetachment of OH^-, the detached electron

comes from a π molecular orbital, which resembles an atomic p orbital on the oxygen atom and is oriented perpendicular to the O-H bond. Therefore, conservation of angular momentum in the photodetachment process predicts the production of an s-wave or a d-wave electron, and for photon energies near threshold the s-wave dominates, resulting in an expected threshold law of $\sigma \sim (E-E_{\rm th})^{1/2}$ for OH^-. However, this prediction does not take into account the electric dipole moment of the molecule. If any long-range potential is present between the products of the photodetachment process, such as the Coulombic potential or a dipole potential, then even the leading term of the expansion describing the cross section is altered. In this case the Wigner law no longer holds and the near-threshold cross section might exhibit a different shape. For photodetachment of OH^-, the anisotropic r^{-2} dipole potential that the departing electron feels plays a key role in determining the threshold behavior. This dipole arises from the mixing of opposite parity states, as will be explained in Sec. III. In addition, because the interaction is dependent on the orientation of the dipole, one might expect that the rotational motion of the molecule will have an effect on the threshold behavior. As one approaches threshold, the photodetached electrons depart on a time scale that is long compared to the rotational period of the molecule giving rise to some rotational averaging of the long-range forces. Therefore, the near-threshold region of the cross section should show the strongest influence from rotational motion [3]. Thus, the threshold photodetachment of OH^- is an experiment in which the coupling of electronic and nuclear motion cannot be neglected.

To gain further insight into what can be learned from photodetachment experiments, consider the similarities between photodetachment of a negative ion and electron-molecule scattering experiments. Photodetachment of a negative ion is essentially equivalent to the second half of an electron-atom inelastic collision with only a limited number of partial waves accessible due to the conservation of angular momentum [15]. An advantage that photodetachment experiments have over electron scattering experiments is that the optical resolution attained through the use of lasers is typically several orders of magnitude higher than the energy resolution of scattering experiments.

In addition to providing information on long-range interactions, determination of the threshold law for an individual threshold allows precise determination of the threshold frequency. For OH^-, these individual thresholds correspond to transitions between the various rotational states of the ion and the neutral molecule. Therefore, the photodetachment experiment provides rotational level information and, in addition, is currently the most precise method for determining electron affinities. The threshold photodetachment technique has been used to determine this quantity for a number of atoms and molecules [1,2,10,11,16–18].

II. EXPERIMENT

The coaxial laser-ion beam spectrometer used for these experiments has been described in detail elsewhere [19,20], so only a brief overview and discussion of recent modifications will be given. The ion beam apparatus has three main regions: the source region, the collimation region, and the coaxial interaction region. Recently, a continuous, effusive ion source was converted to a pulsed free jet expansion source to provide rotational cooling. Typical rotational temperatures with this source were 150 to 250 K as estimated from Boltzmann fits of the intensities of several thresholds. The expansion is crossed with a 1-keV beam of electrons to initiate the formation of ions. A typical time-averaged OH^- current of 10 pA (measured in the interaction region) is produced by expanding a mixture of 10% NH_3, 90% Ne, and a trace of H_2O through a pulsed valve (General Valve Series 9) using a total backing pressure of two atmospheres. The valve is typically operated at 50 Hz with a duty cycle of approximately 1%. The probable mechanism for formation of OH^- is dissociative electron attachment to NH_3 to form NH_2^-. Then, collision of NH_2^- with H_2O results in proton abstraction, forming OH^-. After ion formation, the ion beam is mass selected with a 90° sector magnet, collimated in the second region of the apparatus, and then bent another 90° into the interaction region with an electrostatic quadrupole deflector. As the ions travel from the source region to the interaction region, they are accelerated across a $\sim$2-kV potential difference. This acceleration provides kinematic compression of the velocity spread of the ion beam [21] in order to reduce the effect of Doppler broadening.

In the interaction region, the ion beam interacts coaxially with the laser beam over a 30-cm path length. Photodetached electrons are steered with a weak magnetic field ($\approx$2 G) to a channeltron particle multiplier operated in a pulse counting mode. The weak magnetic field provides discrimination against higher-energy electrons. These higher-energy electrons, originating from lower-lying open channels, increase the scatter in the data. The rotational cooling of the ions also helped eliminate some of this contribution to the electron signal. Gated detection of the electron signal, synchronized with the pulsed valve timing, is employed to increase the signal-to-noise ratio. The electron signal is normalized to the product of the laser power and ion beam current at each frequency. This normalized electron signal, once the prethreshold background has been subtracted, is proportional to the state-selected partial photodetachment cross section near threshold.

A home-built ring dye laser employing DCM dye and pumped by all visible lines of an Ar^+ laser was used for all of the high-resolution scans. Doppler broadening due to the residual velocity spread of the ion beam is $\approx$10 MHz, while the laser linewidth, when operated in its highest-resolution configuration, is $\approx$1–5 MHz. Therefore, the instrumental resolution is limited by the Doppler broadening. The laser wavelength is measured using a wave meter (traveling Michelson interferometer) [22] utilizing a polarization-stabilized He-Ne laser as the reference [23]. The wavelengths measured with the wave meter are corrected for the refractive index of air and the Doppler shift of the ion beam to obtain absolute vacuum wavelengths. For the data presented below the point spacing is either 0.01 or 0.001 cm^{-1}.

III. RESULTS AND DISCUSSION

A. Spectroscopy

Before presenting the photodetachment data, a brief description of the pertinent energy levels will be given. The

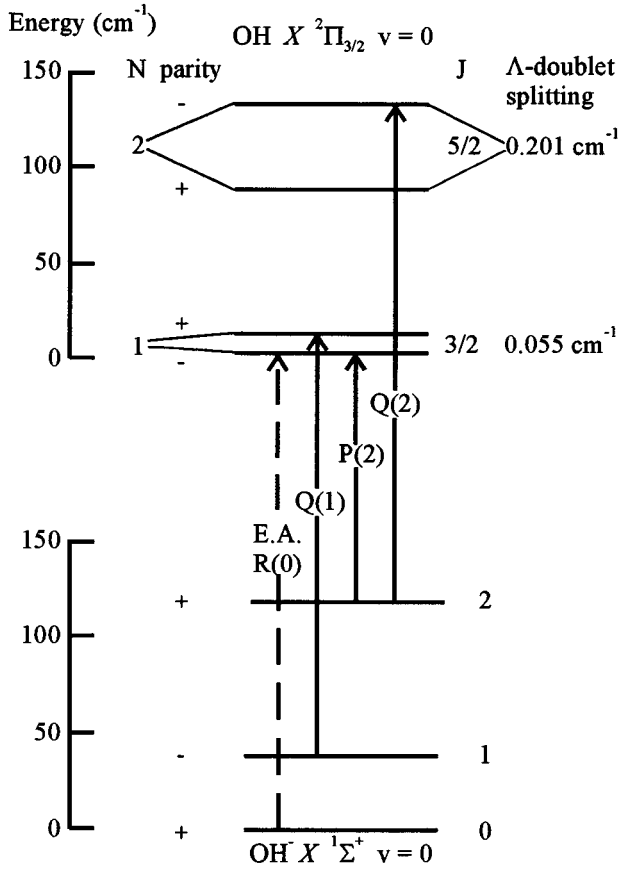

FIG. 1. OH^- and OH rotational energy-level diagram showing the transitions examined in this work. In addition, the transition corresponding to the electron affinity is indicated with a dashed arrow. The Λ-doubling splittings have been exaggerated by a factor of 200. See the text for an explanation of the labels.

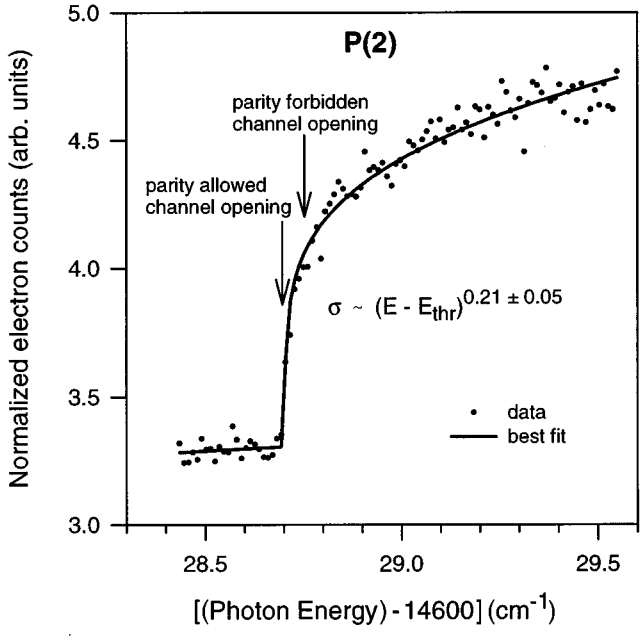

FIG. 2. $P(2)$ threshold for approximately 1 cm^{-1} above threshold with a point spacing of 0.01 cm^{-1}. Photon energy is given in units of wave numbers. The solid line is a best fit to the data using the function shown. Without resolution of the Λ doubling the cross section is seen to rise much sharper than the one-half power predicted by the Wigner threshold law. The power-law exponent of 0.21 ± 0.05 agrees qualitatively with the 0.30 prediction of Engelking's close-coupling model.

transitions examined in this work were transitions from the $X\ ^1\Sigma^+\ v=0$ state of OH^- to the $X\ ^2\Pi_{3/2}\ v=0$ state of neutral OH. The individual thresholds that appear in the photodetachment spectrum correspond to the various allowed transitions between the rotational states of the negative ion and the neutral species. The Λ-type doubling splits the normal twofold degeneracy of the $^2\Pi_{3/2}$ rotational states. This splitting arises from the two possible orientations of the $p\pi$ orbital of the OH molecule relative to the plane of rotation [24] and increases with increasing J (total angular momentum quantum number) for the $^2\Pi_{3/2}$ electronic state. The Λ doubling plays a key role in determining the interaction between the neutral molecule and the departing electron and will be discussed further below. Threshold data were obtained for each of the transitions over an energy range considerably greater than the Λ-doublet splitting, but with resolution much better than the splitting.

The transitions investigated in this work, as well as the transition corresponding to the electron affinity of OH, are indicated on the energy-level diagram of Fig. 1. An assignment of the photodetachment spectrum of OH^- over a range of 650 cm^{-1} above the onset for photodetachment was performed by Schulz *et al.* [3]; therefore, identification of a transition was straightforward. The energy levels are labeled with quantum numbers J and N, and total parity. The total angular momentum is J and the angular momentum neglecting spin is given by N. For closed-shell OH^-, J and N are the same, while for open-shell neutral OH, they differ by one-half. The transitions are labeled with a letter that indicates the rotational branch using the usual notation and a number in parentheses that indicates the initial N of the OH^-. As is the case for neutral molecules, selection rules involving angular momentum and parity govern which photodetachment transitions are allowed [3]. The photon has unit angular momentum, while the detached electron has $\frac{1}{2}$ unit of spin angular momentum. Therefore, the allowed transitions consist of $\Delta J = \frac{3}{2}, \frac{1}{2}, -\frac{1}{2}$, or $-\frac{3}{2}$. Of particular importance for the results obtained below is the parity selection rule, which results in transitions between states of opposite parity for s-wave electrons, which have even parity. Transitions to the other Λ-doublet component are allowed via p-wave electrons and must be very weak near threshold.

B. Electron-OH dynamics

High-resolution scans of the $P(2)$ and $Q(1)$ thresholds, which access opposite-parity Λ-doublet components of the $N=1$ state of $X\ ^2\Pi_{3/2}$ of OH, are shown in Figs. 2 and 3. Examination of the near-threshold scaling of the cross section (threshold law) for the two thresholds reveals interesting results, which can be interpreted in terms of the electron-OH

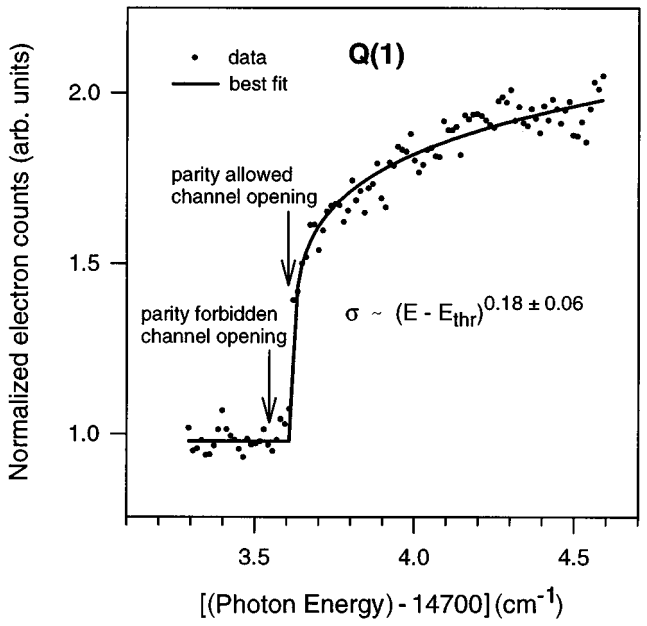

FIG. 3. $Q(1)$ threshold for approximately 1 cm^{-1} above threshold with a point spacing of 0.01 cm^{-1}. Photon energy is given in units of wave numbers. The solid line is a best fit to the data using the function shown. As for the $P(2)$ threshold, non-Wigner scaling of the cross section is observed due to the long-range charge-dipole interaction. The power-law exponent of 0.18 ± 0.06 agrees qualitatively with the close-coupling prediction and is the same as the $P(2)$ exponent within error limits.

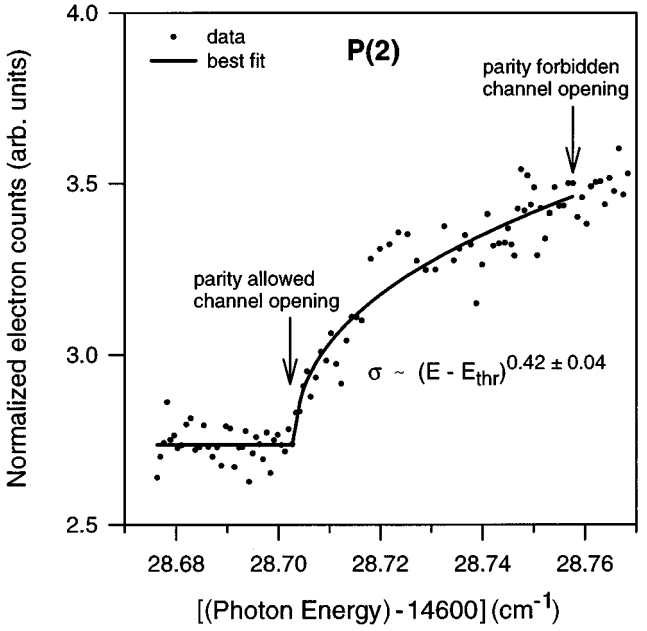

FIG. 4. $P(2)$ threshold once again, this time for approximately 0.06 cm^{-1} above threshold with a point spacing of 0.001 cm^{-1}. Photon energy is given in units of wave numbers. The solid line is a best fit to the data using the function shown. With resolution of the Λ doubling, the scaling of the cross section essentially agrees with the one-half power predicted by the Wigner threshold law.

dynamics. The cross-section data in these figures were fit as follows. First, the prethreshold energy data were least-squares fit by the form

$$\sigma = A + BE, \tag{1}$$

where σ is the cross section, E is the photon energy, and A and B are free parameters. Then, once the prethreshold background has been fit, the post-threshold energy data were least-squares fit by the form

$$\sigma = A + BE + C(E - E_{\mathrm{th}})^D, \tag{2}$$

where E_{th} is the threshold energy for the specific channel opening, C and D are free parameters, and A and B are kept fixed at the values determined from fitting the prethreshold background. E_{th} was not left as a free parameter, but rather was varied over a reasonable range, and the residuals closest to threshold were examined for any systematic trends. Note that E_{th} for the two thresholds was determined from the data in Figs. 4 and 5, which had a smaller point spacing (0.001 cm^{-1}) than the data in Figs. 2 and 3. The most important parameter of the fits is the power-law exponent, since theory makes specific predictions about its value, whereas the other parameters are simply scaling parameters that depend on the experimental conditions. The uncertainty given for the power-law exponent was determined by varying this parameter, while keeping the other parameters constant, until the χ^2 of the fit was doubled. These uncertainties are an approximation of the 95% confidence limits.

The results of the fits can be described in terms of the dynamics of the interaction between the departing electron and the neutral OH molecule. Figures 2 and 3 show the $P(2)$ and $Q(1)$ thresholds, respectively, for approximately 1 cm^{-1} above threshold. The data clearly rise more sharply than would be expected from the one-half power predicted by the Wigner threshold law. This deviation from the Wigner law is not unexpected, as several theoretical studies have

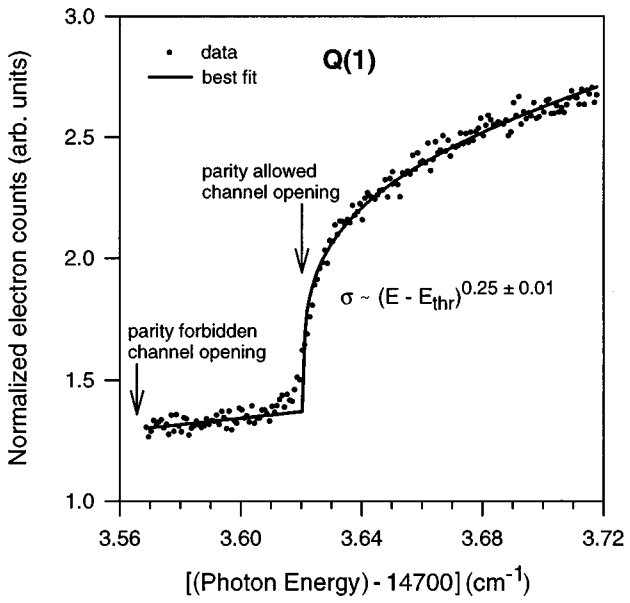

FIG. 5. $Q(1)$ threshold once again, this time for approximately 0.10 cm^{-1} above threshold with a point spacing of 0.001 cm^{-1}. Photon energy is given in units of wave numbers. The solid line is a best fit to the data using the function shown. Non-Wigner scaling is observed; see text for explanation.

predicted a sharper rise [25–27] and experimental studies have confirmed this effect for OH^- [3,28,29] as well as CH_3S^- [30]. The results of this work provide further confirmation of this effect. Rau pointed out that repulsive potentials, such as the centrifugal potential, cause suppression of the near-threshold cross section, while attractive potentials enhance it [31]. This sharper rise comes about because the underlying assumption of the Wigner threshold law is violated for an OH molecule possessing a dipole moment. This dipole moment produces an anisotropic r^{-2} interaction potential between the detached electron and the molecule; therefore, the centrifugal potential is no longer the longest-range interaction. Gailitis and Damburg [26] and O'Malley [25] have derived a threshold law for photodetachment based on a spherically symmetric long-range potential, $V(r) = -ed/r^2$, where e is the electron charge and d is a constant. However, the true interaction is dependent on the orientation of the dipole and thus contains a cos θ angular dependence. Engelking has proposed a model of strong coupling between an electron and a rotating dipole that takes into account the angular dependence and gives specific predictions for power-law exponents for the OH molecule in various rotational states [27,32]. These predictions can be directly compared with our experimental results. The $P(2)$ and $Q(1)$ thresholds both leave the OH in $J=3/2$ of $^2\Pi_{3/2}$ and give power-law exponents of 0.21 ± 0.05 and 0.18 ± 0.06, respectively, from best fits to the data that cover a range of approximately 1 cm^{-1} above threshold, while the strong-coupling model predicts [27,29] $\sigma\sim(E-E_{th})^{0.301}$. While the agreement between the experiment and the prediction is not quantitative, there is good qualitative agreement. It should be noted that the fits cover a range that is much larger than the Λ-doublet splitting. Within experimental uncertainty, the results of the fits for $P(2)$ and $Q(1)$ are the same, which is consistent with the idea that the interaction between the final rotational state of the neutral OH molecule and the departing electron governs the threshold behavior. In fact, earlier work has shown that the $P(2)$, $Q(1)$, and $R(0)$ thresholds all have the same shape when viewed over a 2.5-cm^{-1} range [3].

Up to this point, the effect of the Λ doubling of the OH states on the threshold cross section has been neglected; this splitting will now be included. Figure 4 shows the $P(2)$ threshold once again, however, in this figure the data point spacing is now 0.001 cm^{-1} and the data only extend for approximately 0.06 cm^{-1} above threshold. On this energy scale, the Λ-doublet splitting for the $J=3/2$ $^2\Pi_{3/2}$ state of OH, 0.055 cm^{-1} [33], is well resolved. The splitting can be observed in Fig. 4 as the difference between the photon energies marked as parity-allowed channel opening and parity-forbidden channel opening. Significantly different threshold behavior is observed depending on the range covered by the data. A best fit to the data in Fig. 4 over a 0.05-cm^{-1} range, using the procedure described above, gives a power-law exponent of 0.42 ± 0.04 compared to the 0.21 ± 0.05 determined for the same threshold from the fit over a 1-cm^{-1} range shown in Fig. 2. It should be noted that the range of the fit for Fig. 4 is equal to the Λ-doublet splitting. Earlier work [3] has shown that the shape of the $P(9)$ threshold of OH^- is adequately described by a power-law exponent of one-half over a range equal to the Λ-doublet splitting (≈ 3 cm^{-1}) for that final state of OH. When the Λ doubling is resolved, the cross section is seen to rise more gradually for both of these P-branch thresholds, producing a scaling that is much closer to the prediction of the Wigner law.

The different behaviors of the near-threshold cross section for the same rotational threshold can be understood by considering the Λ doubling and the origin of the dipole moment in OH that gives rise to the r^{-2} interaction potential. The Λ-doublet states are states of definite parity, with the two components having opposite parity [24]. Absorption of a near-threshold photon by OH^- produces an s-wave electron having even parity, thereby leaving the OH molecule in a state of opposite parity to the initial OH^- state [3]. Therefore, as is shown in Fig. 1, the $P(2)$ threshold leaves the OH molecule in an odd-parity state, which is the lower state of the Λ doublet for this particular rotational level [33]. In contrast, the $Q(1)$ transition terminates on the same rotational level, but populates the other Λ-doublet level. Any state having definite parity cannot possess a dipole moment, since the dipole moment operator has odd parity and thus the dipole moment integral will vanish. Therefore, in the limit that photodetachment leaves the OH molecule in a state of definite parity, there is no dipole moment that can give rise to a r^{-2} dipole potential, and, therefore, the threshold behavior would be expected to obey the Wigner law. This limiting behavior explains the gradual rise of the cross section in Fig. 4, which is in reasonable agreement with the Wigner law prediction of one-half.

However, the above explanation does not account for the sharper rise observed in Fig. 2. The exact origin of the dipole of OH must now be considered. For a detached electron moving slowly compared to the rotational period of the molecule, angular momentum exchange between the polar molecule and the electron can occur [27], thereby leading to an exchange of energy between the molecule and the electron. If the kinetic energy of the free electron is greater than the Λ-doublet splitting, this interaction between the electron and the molecule could mix the Λ-doublet components of a given rotational level of the OH molecule to produce two degenerate states lacking definite parity [28]. For these mixed-parity states, the dipole moment integral would no longer vanish, thus giving rise to a dipole moment; in other words, the electric field due to the detached electron causes a perturbation giving rise to an effective dipole moment in the OH molecule. Mixing of the degenerate ℓ states of atomic hydrogen (e.g., $2s$ and $2p$) produces a dipole moment in an analogous manner [34]. Another possible source of mixed-parity states for OH is mixing of different rotational levels of opposite parity; however, the electron kinetic energies covered by the data presented in this paper are not large enough to cause this type of mixing. For the data shown in Fig. 2, the detached electrons have enough energy to mix the Λ-doublet components, except for the 5 or 6 points closest to threshold, thus explaining the sharp deviation from Wigner behavior. No evidence of a kink in the cross section is seen at the photon energy corresponding to the opening of the parity-forbidden Λ-doublet component, although this is not surprising considering the relatively large (0.01 cm^{-1}) frequency spacing of the data.

Another view of the origin of the dipole moment in OH may be gained by considering the relationship between rota-

tional motion and a dipole moment. A dipolar rotor lacking a component of angular momentum along the dipole axis will rotate about an axis perpendicular to the dipole axis, thus averaging out the projection of the dipole moment in the laboratory-fixed coordinate system. It is the projection of the dipole moment in this coordinate system, and not the molecular-fixed coordinate system, that defines a dipole moment [35]. On the other hand, a dipolar rotor with a component of angular momentum along the dipole axis will precess about the space projection of the total angular momentum in order to conserve the component along the dipole axis. Therefore, the field from the dipole does not average out, giving rise to a permanent projection in the laboratory-fixed coordinate system, or, in other words, a dipole moment. In the case of $^2\Pi$ OH, the component of angular momentum along the dipole axis is the orbital electronic angular momentum (Λ) and the states that have this component are the degenerate mixed-parity states. However, the Λ doubling removes this degeneracy and produces states of definite parity, which no longer conserve the angular momentum along the dipole axis. Therefore, cross-section data that resolve the Λ doubling, such as the data shown in Fig. 4, would exhibit Wigner behavior for the lower-energy channel in the limited energy region before the higher Λ-doublet channel opens [36].

Figure 5 shows the $Q(1)$ threshold for approximately $0.1\ \mathrm{cm}^{-1}$ above the threshold frequency, a much smaller range than that covered by the data shown in Fig. 3. Since the point spacing of the data shown in Fig. 5 is $0.001\ \mathrm{cm}^{-1}$ and the Λ-doublet separation is well resolved under this resolution, one might expect Wigner law scaling of the cross section for these data. However, the power-law exponent determined from a best fit to these data is 0.25 ± 0.01. Thus, non-Wigner behavior starts even for very small energies above threshold for this transition, which suggests that the electron mixes the opposite-parity states even though it has little kinetic energy. Similar non-Wigner behavior is observed in photodetachment data for the $Q(2)$ transition. Although the quality of the fit was poor due to a large amount of scatter in the data, a power-law exponent of ≈0.2 was obtained from a fit covering $0.1\ \mathrm{cm}^{-1}$ above threshold.

The power-law exponents for both scans of the $Q(1)$ threshold, which have different ranges above threshold, have overlapping experimental uncertainties. The range of the fit for the data in Fig. 5 was truncated several times to as low as $0.01\ \mathrm{cm}^{-1}$ above threshold. It was found that the power-law exponent remained essentially unchanged. In addition, earlier low-resolution Q-branch threshold cross-section data for OH^- where the different Q-branch transitions were not resolved, was well represented by a power-law exponent of 0.25 over a range of $100\ \mathrm{cm}^{-1}$ [6]. Therefore, for these Q-branch transitions, which always terminate in the upper component of the Λ doublet for transitions to the $\frac{3}{2}$ spin-orbit electronic state, it appears that $(E-E_{\mathrm{th}})^{0.25}$ describes the cross section for 0.01 to $100\ \mathrm{cm}^{-1}$ above threshold. In contrast, for P-branch transitions, which terminate in the lower component of the Λ doublet, the apparent threshold law depends on whether the range of the fit is larger or smaller than the Λ-doublet splitting, and is Wigner-like if the range of the fit is within the Λ-doublet splitting of threshold. For larger ranges, the threshold law is closer to that observed for the Q-branch transitions.

Engelking has performed calculations to investigate the effect of the Λ doubling upon the threshold behavior [36]. Although the calculations were performed for the transition that terminates in the $J=\frac{1}{2}$ state of OH, the results should apply qualitatively to the $Q(1)$ and $P(2)$ thresholds [29], which terminate in the $J=\frac{3}{2}$ state. It was found that the threshold behavior is described by two cases [36]. One case occurs when s-wave detachment to the lower Λ-doublet component is forbidden by the parity selection rule. This case applies to the $Q(1)$ threshold; the photon energy that corresponds to the transition to the lower Λ-doublet component is marked as the parity-forbidden channel opening. The calculation for this case predicts weakly allowed p-wave detachment, given by $(E-E_{\mathrm{th}})^{3/2}$, for photon energies above the lower channel opening, but below the channel opening corresponding to the transition to the upper Λ-doublet component. As the photon energy is increased through the upper channel opening, Engelking predicts that the threshold law abruptly reverts to the strong-coupling prediction of $(E-E_{\mathrm{th}})^{0.301}$. The data in Fig. 5 qualitatively agree with the predictions of the calculation, as the cross section exhibits a slow rise prior to the parity-allowed channel opening, followed by the abrupt rise given by $(E-E_{\mathrm{th}})^{0.25}$. The other case, which applies to the $P(2)$ threshold, occurs when s-wave detachment to the lower Λ-doublet component is allowed. For this case, the calculation predicts Wigner law behavior for photon energies less than the upper channel opening, followed by a gradual conversion to a non-Wigner sharper rise. The $P(2)$ data in Figs. 2 and 4 are consistent with this prediction.

It was thought that resonances or some interference structure due to autodetaching dipole-bound states might appear in the photodetachment spectrum of OH^-, as has been observed for other negative ions [37–42]. However, no evidence of any resonance structure was observed near the thresholds scanned in this work. The dipole moment of OH^- is 166 D, which exceeds the minimum dipole strength required to bind an electron in the field of a point dipole [43]. However, Garrett showed that the inclusion of rotational motion and the finite size of the dipole increases this critical dipole binding strength to ≈2 D [44].

C. Electron affinity

Although the threshold corresponding to the electron affinity was not scanned, the extremely high resolution of laser photodetachment threshold spectroscopy and the technique of combination differences allows the accurate determination of the electron affinity of OH. Fitting of the experimental cross-section data for the photodetachment thresholds provides the threshold frequencies for transitions between specific rotational states of the negative ion and the neutral molecule, as well as power-law exponents as discussed above. In contrast to photoionization experiments, the apparent onset of electron detachment really indicates the transition frequency without concern about Rydberg states [2], allowing the accurate determination of spectroscopic quantities.

TABLE I. Threshold frequencies and spectroscopic results from this work and comparison with prior results. All values are in cm^{-1} and uncertainties were determined as explained in the text.

	This work	Schulz *et al.*[a]	Rosenbaum *et al.*[b]	Engelking[c]
ν $Q(1)$	14 703.62(2)			
ν $P(2)$	14 628.70(3)			
$B_0(OH^-)$	18.732(3)	18.741(4)	18.7350(4)	
$E_A(OH)$	14 741.02(3)	14 741.0(2)		14 740.8(2)

[a]Reference [3].
[b]Reference [4].
[c]Reference [29].

The $Q(1)$ and $P(2)$ thresholds terminate on different Λ-doublet components of the same rotational state of neutral OH, but originate from different rotational states of OH^-. Therefore, the difference of the threshold frequencies of $Q(1)$ and $P(2)$ is related to the rotational constant of the negative ion but not the neutral OH. Knowledge of the OH^- rotational constant and one of the threshold frequencies can be combined to determine the electron affinity of OH. Specifically, the rotational energy of OH^- in the vibrational ground state relative to $J=0$ is

$$E(J)=B_0J(J+1)-D_0J^2(J+1)^2, \tag{3}$$

where B_0 is the rotational constant, D_0 is the centrifugal distortion constant, and higher-order terms are ignored. Using the above expression, the difference in the transition frequencies of $Q(1)$ and $P(2)$ can written as

$$\nu_{Q(1)}-\nu_{P(2)}=4B_0-32D_0+\Delta F(3/2), \tag{4}$$

where $\Delta F(3/2)$ is the Λ-doubling splitting in the upper state of the transitions ($J=3/2$), and is 0.055 cm^{-1} [33]. The transition frequencies of $Q(1)$ and $P(2)$, determined from fits to the data of Figs. 4 and 5, are 14 703.621 and 14 628.703 cm^{-1}, respectively. Using these frequencies, the value of the centrifugal distortion constant for OH^- determined by Schulz and co-workers, $2.052(45)\times10^{-3}$ cm^{-1} [3], and Eq. (4) gives 18.732 cm^{-1} for B_0. Then, using Eq. (3) and Fig. 1, the electron affinity of OH can be written as

$$E_A(OH)=\nu_{Q(1)}+2B_0-4D_0-\Delta F(3/2). \tag{5}$$

The $Q(1)$ transition frequency was used to determine the electron affinity because the uncertainty in this transition was slightly smaller than for $P(2)$, as will be discussed below. The electron affinity of OH, as determined from the above equation and threshold frequency, is 14 741.02 cm^{-1}. Table I summarizes the threshold frequencies and spectroscopic results that were obtained from this work including experimental uncertainties, and lists some results from prior experiments for comparison.

The primary source of uncertainty in the determination of $B_0(OH^-)$ and $E_A(OH)$ is uncertainty in the threshold frequencies, which has several significant sources. Uncertainty in the reproducibility of the wave meter readings was estimated to be ±0.002 cm^{-1}. In addition, a large portion of the uncertainty in the threshold frequencies can be attributed to uncertainty in the wavelength calibration of the polarization-stabilized He-Ne laser used as the reference for the wave meter. Although this uncertainty is systematic, its effect, as well as any long-term drift of the He-Ne laser frequency, was approximated by adding an uncertainty of half the longitudinal mode spacing of the He-Ne laser, ±0.019 cm^{-1}, to the uncertainties of the threshold frequencies. In addition to the above sources, there is also an uncertainty from the least-squares fitting procedure; as was done for the power-law exponents, this uncertainty was determined by doubling the χ^2 of the fit. For $Q(1)$ this uncertainty is ±0.002 cm^{-1}, while for $P(2)$ it is ±0.006 cm^{-1}. The above uncertainties were added to obtain the uncertainties in each of the threshold frequencies, which are given in Table I. Propagation of the uncertainties in the transition frequencies through the calculations to determine the rotational constant and electron affinity gives the final uncertainties for those quantities, which are also shown in Table I.

As is shown in Table I, the most accurate determination of $B_0(OH^-)$ was performed by Rosenbaum *et al.*, using velocity modulation laser spectroscopy [4]. The uncertainty in $E_A(OH)$, ±0.03 cm^{-1}, is the most accurate determination to date by about an order of magnitude better than previous work [3,29]. To determine the electron affinity more accurately than the result reported in this work would require scanning the rotational threshold corresponding to the electron affinity, $R(0)$, with both copropagating and counterpropagating laser-ion beam geometries and then taking the geometrical average of the two apparent threshold frequencies [45,46].

IV. CONCLUSIONS

Laser photodetachment threshold spectroscopy was used to investigate rotational thresholds of OH^- under high resolution. For the $P(2)$ threshold it was found that the apparent energy dependence of the photodetachment cross section depends on the range of data above threshold included in the fit. On the other hand, for the $Q(1)$ threshold the energy dependence was the same for all ranges that were investigated. These results were interpreted by considering the relationship of the Λ doubling and the long-range interaction between the neutral OH and the departing electron. The cross section rises faster than the Wigner law $(E-E_{th})^{1/2}$ prediction when a r^{-2} dipole potential is present between the electron and the neutral. In addition, an electron affinity of 14 741.02(3) cm^{-1} for OH was determined from the frequencies of two rotational thresholds.

ACKNOWLEDGMENTS

Support for this research was generously provided by the National Science Foundation through Grants No. PHY95-12150 and No. CHE93-18639 and by AFOSR through the AASERT program. The authors thank Dr. Sean M. Casey for helpful discussions and a critical reading of the manuscript. The authors also thank Professor Paul C. Engelking for useful discussions.

[1] R. D. Mead, A. E. Stevens, and W. C. Lineberger, in *Gas Phase Ion Chemistry*, edited by M. T. Bowers (Academic Press, New York, 1984), Vol. 3, p. 213.
[2] C. Blondel, Phys. Scr. **T58**, 31 (1995).
[3] P. A. Schulz, R. D. Mead, P. L. Jones, and W. C. Lineberger, J. Chem. Phys. **77**, 1153 (1982).
[4] N. H. Rosenbaum, J. C. Owrutsky, L. M. Tack, and R. J. Saykally, J. Chem. Phys. **84**, 5308 (1986).
[5] E. P. Wigner, Phys. Rev. **73**, 1002 (1948).
[6] H. Hotop, T. A. Patterson, and W. C. Lineberger, J. Chem. Phys. **60**, 1806 (1974).
[7] J. W. Farley, Phys. Rev. A **40**, 6286 (1989).
[8] H. Hotop, T. A. Patterson, and W. C. Lineberger, Phys. Rev. A **8**, 762 (1973).
[9] W. C. Lineberger and B. W. Woodward, Phys. Rev. Lett. **25**, 424 (1970).
[10] D. Hanstorp and M. Gustafsson, J. Phys. B **25**, 1773 (1992).
[11] G. Haeffler, D. Hanstorp, I. Kiyan, A. E. Klinkmüller, U. Ljungblad, and D. J. Pegg, Phys. Rev. A **53**, 4127 (1996).
[12] L. M. Branscomb, D. S. Burch, S. J. Smith, and S. Geltman, Phys. Rev. **111**, 504 (1958).
[13] S. Geltman, Phys. Rev. **112**, 176 (1958).
[14] K. J. Reed, A. H. Zimmerman, H. C. Andersen, and J. I. Brauman, J. Chem. Phys. **64**, 1368 (1976).
[15] W. C. Lineberger, H. Hotop, and T. A. Patterson, in *Electron and Photon Interactions with Atoms*, edited by H. Kleinpoppen and M. R. C. McDowell (Plenum, New York, 1976), p. 125.
[16] U. Berzinsh, M. Gustafsson, D. Hanstorp, A. Klinkmüller, U. Ljungblad, and A.-M. Mårtensson-Pendrill, Phys. Rev. A **51**, 231 (1995).
[17] K. R. Lykke, K. K. Murray, and W. C. Lineberger, Phys. Rev. A **43**, 6104 (1991).
[18] P. S. Drzaic, J. Marks, and J. I. Brauman, in *Gas Phase Ion Chemistry*, edited by M. T. Bowers (Academic, New York, 1984), Vol. 3, p. 167.
[19] U. Hefter, R. D. Mead, P. A. Schulz, and W. C. Lineberger, Phys. Rev. A **28**, 1429 (1983).
[20] R. D. Mead, Ph.D. thesis, University of Colorado, 1984 (unpublished).
[21] W. Demtröder, *Laser Spectroscopy: Basic Concepts and Instrumentation* (Springer-Verlag, Berlin, 1982).
[22] J. L. Hall and S. A. Lee, Appl. Phys. Lett. **29**, 367 (1976).
[23] R. Balhorn, H. Kunzmann, and F. Lebowsky, Appl. Opt. **11**, 742 (1972).
[24] P. Andresen and E. W. Rothe, J. Chem. Phys. **82**, 3634 (1985).
[25] T. F. O'Malley, Phys. Rev. **137**, A1668 (1965).
[26] M. Gailitis and R. Damburg, Proc. Phys. Soc. **82**, 192 (1963).
[27] P. C. Engelking, Phys. Rev. A **26**, 740 (1982).
[28] R. D. Mead, K. R. Lykke, and W. C. Lineberger, in *Electronic and Atomic Collisions*, edited by J. Eichler, I. V. Hertel, and N. Stolterfoht (Elsevier, Amsterdam, 1984), p. 721.
[29] P. C. Engelking (private communication).
[30] B. K. Janousek and J. I. Brauman, J. Chem. Phys. **72**, 694 (1980).
[31] A. R. P. Rau, Comments At. Mol. Phys. **14**, 285 (1984).
[32] D. R. Herrick and P. C. Engelking, Phys. Rev. A **29**, 2421 (1984).
[33] J. A. Coxon, Can. J. Phys. **58**, 933 (1980).
[34] H. A. Bethe and E. E. Salpeter, *Quantum Mechanics of One and Two Electron Atoms* (Plenum, New York, 1957).
[35] W. Klemperer, K. K. Lehmann, J. K. G. Watson, and S. C. Wofsy, J. Phys. Chem. **97**, 2413 (1993).
[36] P. C. Engelking and D. R. Herrick, Phys. Rev. A **29**, 2425 (1984).
[37] A. H. Zimmerman and J. I. Brauman, J. Chem. Phys. **66**, 5823 (1977).
[38] R. L. Jackson, A. H. Zimmerman, and J. I. Brauman, J. Chem. Phys. **71**, 2088 (1979).
[39] R. D. Mead, K. R. Lykke, W. C. Lineberger, J. Marks, and J. I. Brauman, J. Chem. Phys. **81**, 4883 (1984).
[40] T. Andersen, K. R. Lykke, D. M. Neumark, and W. C. Lineberger, J. Chem. Phys. **86**, 1858 (1987).
[41] J. Marks, J. I. Brauman, R. D. Mead, K. R. Lykke, and W. C. Lineberger, J. Chem. Phys. **88**, 6785 (1988).
[42] K. Yokoyama, G. W. Leach, J. B. Kim, and W. C. Lineberger, J. Chem. Phys. (to be published).
[43] E. Fermi and E. Teller, Phys. Rev. **72**, 406 (1947).
[44] W. R. Garrett, Chem. Phys. Lett. **81**, 4883 (1970).
[45] D. M. Neumark, K. R. Lykke, T. Andersen, and W. C. Lineberger, Phys. Rev. A **32**, 1890 (1985).
[46] M. Kaivola, O. Poulsen, E. Riis, and S. A. Lee, Phys. Rev. Lett. **54**, 255 (1985).